Full-Sphere Radiation Pattern Characterization of IoT Devices via Pattern Stitching

Jure Soklič* and Holger Arthaber
Institute of Electrodynamics, Microwave and Circuit Engineering, TU Wien, Vienna, Austria
e-mail: jure.soklic@tuwien.ac.at; holger.arthaber@tuwien.ac.at

Abstract

A full-sphere characterization method based on stitching multiple truncated radiation patterns together has been proposed recently. The method considers classical antenna measurements where both the probe antenna and the antenna under test (AUT) are connected to ports of a vector network analyzer (VNA) via coaxial cables. Such measurements are not always possible, for example, when characterizing radiation patterns of Internet of Things (IoT) devices where the antenna is integrated onto the printed circuit board (PCB) and has no coaxial connector attached. This paper presents the measurement procedure and the required adaptations to the aforementioned method for characterization of such devices. An extensive error analysis is carried out on the obtained results to investigate the performance of the method and identify its limits.

1 Introduction

When dealing with spherical antenna measurements, be it near or far field, the angular range that can be covered in a single measurement is typically limited by the design of the measurement system and the support structure of the antenna under test (AUT). This leads to missing field pattern information and truncation errors, which is especially problematic when characterizing low gain antennas (LGAs). To mitigate the effects of truncation, an iterative pattern processing approach has been proposed in [1, 2]. Recent investigation of the performance of translation and rotation operations on such iteratively processed patterns has shown that the error increase can be kept reasonably low. Therefore, such patterns could serve as a basis for stitching multiple truncated patterns together [3]. This was exploited in [4] to develop a functioning method for stitching truncated patterns of an AUT measured in two orientations, thus obtaining full sphere radiation patterns. The method considers classical antenna measurements where the AUT is equipped with a coaxial connector and direct measurements of S-parameters between the probe antenna and the AUT can be done. The limiting factors of this method in terms of accuracy were found to be the coaxial cable and the AUT's support structure, since their position relative to the antenna changes between measurements in different orientations.

In this paper, battery-powered Internet of Things (IoT) devices are considered, where antennas are integrated onto the printed circuit board (PCB) and have no coaxial connector. By using such devices, changing coaxial cable position between measurements can be avoided. The other dominant source of error from [4] can be minimized by using materials with electromagnetic properties closely resembling those of air for the support structure. This gave an indication that the accuracy of the method could be further improved when characterizing such devices. In order to test the performance, measurements were done on exemplary test objects. A measurement setup for measuring connectorless devices was devised for this purpose and the pattern-stitching method was adapted accordingly. This will be presented in the next sections, followed by the results obtained in an extensive error analysis.

2 Measurement Procedure

Several connectorless battery-powered IoT devices were needed for testing purposes, along with a measurement setup which would allow to measure these devices under test (DUTs) in the anechoic chamber at our university which can cover full 360° range in ϕ and θ angles up to $\theta_{\text{trunc}} = 140°$.

2.1 Test Objects

Four commercially available DUTs of different sizes were used as test objects. All four are equipped with a 2.4 GHz radio transceiver chip and a printed inverted-F antenna. Their dimensions are listed in Table 1. A special firmware

Table 1. Test Objects

test object	width (mm)	length (mm)	height (mm)
DUT 1	48	36	11
DUT 2	67	34	12
DUT 3	104	82	13
DUT 4	175	123	14

for measuring the DUT's performance at eleven frequencies within the 2.4 GHz ISM band was installed on each of them. With this firmware, the DUT operates in the following manner: First, it waits to receive a wake-up signal.

Once received, it transmits a continuous wave (CW) signal with the maximum chip output power of 1 dBm at the first frequency to be measured. It then proceeds to the next frequency, where it again transmits a CW signal of the same power. Following this behavior, it progresses through all eleven measurement frequencies.
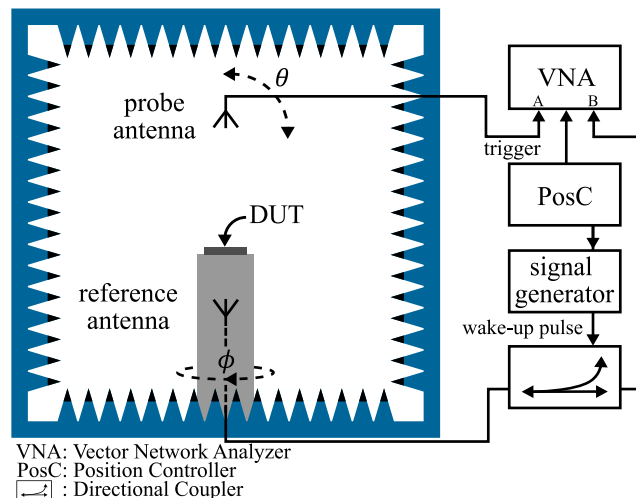
2.2 Measurement Setup

Since classical two-port S-parameter measurements are not possible when characterizing connectorless devices, a modified approach was required. The DUTs were programmed to transmit, thus the probe antenna (Fig. 1a) had to serve as the receiver. A vector network analyzer (VNA) measurement of the incoming wave from the probe (A) would suffice to obtain relative magnitude patterns, but this does not give us coherent phase information, which is needed for the pattern stitching method [4] to work. In order to obtain a reference signal (B) for coherent phase information, an additional antenna had to be used. This reference antenna must always maintain the same distance and orientation with regards to the DUT. Since our anechoic chamber has a theta-over-phi scanning system where the DUT is mounted onto the phi rotary stage, the reference antenna also had to be placed somewhere on the rotary stage. The placement of the antenna is shown in Fig. 1b. The reference antenna was then covered with the support structure on which the DUT was placed, as shown in Fig. 1a. ROHACELL® was used for the support structure because its permittivity closely resembles the permittivity of air.

(a)   **(b)**
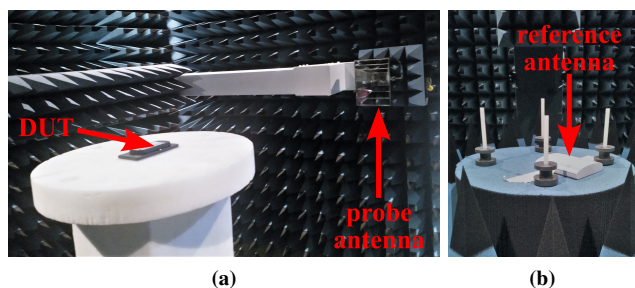
Figure 1. The DUT and the (dual ridge horn) probe antenna (a) and the (circular polarized patch) reference antenna (b) used in the measurements.

During the measurement, the DUT waits for a wake-up pulse before it starts to transmit. Therefore, a wake-up pulse must be sent at every (χ, θ, ϕ) measurement position and the measurements have to be timed precisely. This was achieved in the following manner: When in position, the position controller (PosC) sends a trigger signal to the signal generator, which in turn transmits a CW pulse to the reference antenna. Since the absolute signal levels received by the reference antenna are irrelevant—used only for phase reference—a directional coupler may be used without restrictions to allow to both transmit a wake-up pulse via the reference antenna as well as to measure the signal transmitted by the DUT and received by the reference antenna at

the VNA port. Complete measurement setup with which a phase-coherent ratio measurement (A/B) between the wave incoming from the probe antenna and the wave incoming from the reference antenna was measured with the VNA is shown in Fig. 2.

VNA: Vector Network Analyzer
PosC: Position Controller
⬓ : Directional Coupler

Figure 2. Measurement setup: anechoic chamber.

2.3 Magnitude Calibration

The measurement procedure described up to this point gives coherent phase information but only relative signal levels. To determine parameters such as equivalent isotropic radiated power (EIRP) or total radiated power (TRP), an additional measurement is required. While classical two-port measurements allow for gain calibration by substituting the AUT with a standard gain horn (SGH) with known gain, this is not possible in the case of connectorless test objects. Instead, the absolute power received by the probe antenna at an arbitrary point, $(\chi_0, \theta_0, \phi_0)$, is measured. Since the DUT transmits short pulsed CW signals, a spectrum analyzer (SA) had to be used instead of a power meter. The EIRP can then be derived from the link budget equation:

$$\text{EIRP} = P_{\text{SA}} + \text{ATT} - G_{\text{probe}} + \text{FSPL} \qquad (1)$$

In (1), P_{SA} is the power measured with the spectrum analyzer, ATT represents both the cable losses on the path from probe antenna to the SA and the SA power correction factor, G_{probe} is the probe gain and FSPL the free-space path loss between the DUT and the probe antenna. Once the EIRP is known, the magnitude of the electric field at the measurement distance d can be calculated:

$$|E_d(\chi_0, \theta_0, \phi_0)| = \sqrt{\frac{2Z_0 \cdot 10^{\frac{\text{EIRP}}{10}}}{4\pi d^2}} \qquad (2)$$

Finally, the known value of $|E_d|$ at $(\chi_0, \theta_0, \phi_0)$ can be compared to the relative magnitude measured at that same position during the probe/reference relative measurement in order to obtain a correction factor which can then be applied to all measurement points. This has to be done separately for each (truncated) measurement.

3 Pattern Stitching Method Adaptation

In accordance with the range limits of our anechoic chamber ($\theta_{\text{trunc}} = 140°$), the DUT needs to be measured in two orientations to obtain full-sphere patterns. When changing the orientation, the signals received at both the probe and the reference antenna also change. As mentioned earlier, the magnitude of each measurement is calibrated by measuring the signal power received by the probe antenna at a single measurement point. Ideally, this would bring the two measurements to matching magnitude levels. However, it was observed that this single-point calibration procedure can cause a significant increase of the weighted scaled mean square error (SMSE)[1] in the overlapping region when bad calibration points are chosen, i.e., points where the antenna radiates poorly. Moreover, the magnitude calibration does not correct for the change in phase between the measurements which occurs because the antenna is turned over.

To tackle these issues, the alignment procedure was modified. Specifically, the SMSE minimization procedure had to be extended by two additional parameters. Parameter m represents the magnitude mismatch, while ψ stands for the phase difference between the two measurements. The radiation pattern of one measurement is then modified in the following simple manner:

$$E_{\text{corrected}}(\chi, \theta, \phi) = m \cdot E(\chi, \theta, \phi) \cdot e^{-j\psi} \qquad (3)$$

With these adjustments, the method is now capable of compensating for both the magnitude and the phase offset between two measurements during the alignment procedure.

4 Error Analysis

All DUTs were measured as described in Section 2 and stitched together with the adapted method from Section 3. These full-sphere patterns were then analyzed in terms of errors, as will be shown in the following subsections.

4.1 Mismatch in the Overlapping Region

Already during stitching, the weighted SMSE in the overlapping region was evaluated to see how well the truncated measurements can be matched. The mean and maximum values over all frequency channels are shown in Table 2, along with the values of the two AUTs presented in [4]. To our surprise, the weighted SMSE values of the smaller two DUTs are only a few decibel lower than those of the cable-connected AUTs, while the weighted SMSE values of the larger two are in the same range as the results for the 2-port measurement of the UWB antenna. This implies that even a low permittivity ROHACELL® support structure has a much larger influence on the pattern than first expected.

---

[1]In [3, 4], normalized mean square error (NMSE) was used to represent $\frac{1}{N}\sum_{\chi,\theta,\phi} |x - x_{\text{est}}|^2 / \max_{\chi,\theta,\phi} |x|^2$, which is not the standard definition. To avoid using conflicting definitions, this same metric has been called scaled mean square error (SMSE) in this work, but results reported as NMSE in [3,4] can be directly compared to SMSE values of this paper.

Table 2. Weighted SMSE in the Overlapping Region

test object	weighted SMSE (dB)	
	mean	**max**
DUT 1	–27.83	–27.22
DUT 2	–28.58	–27.52
DUT 3	–24.36	–23.19
DUT 4	–23.94	–22.40
folded dipole[1] [4]	–21.09	–19.93
UWB antenna[1] [4]	–24.37	–21.59

4.2 Stitched Full-Sphere Pattern Error

An SMSE analysis was carried out to evaluate how well the stitched full-sphere patterns match the measurement data. Since radiation patterns obtained with a single full-sphere measurement were not available for our DUTs, the following approach was used for the analysis:

- *top (hemisphere)* — Fixed during the stitching procedure, stitched patterns up to θ_{trunc} could be compared with measured data directly.

- *bottom (hemisphere)* — Translated, rotated, scaled and phase-shifted during stitching, thus the spherical wave coefficients (SWCs) of stitched patterns had to be reversed back to the initial coordinate system, magnitude and phase before being compared with measured values up to θ_{trunc}.

The mean and maximum SMSE values over all measured frequencies are listed in Table 3 for both *top* and *bottom* measurements. These errors are more than 20 dB

Table 3. SMSE Analysis Results

| test object	measurement	SMSE (dB)	
		mean	**max**
DUT 1	*top*	–30.10	–29.62
	bottom	–30.41	–30.10
DUT 2	*top*	–30.96	–29.80
	bottom	–31.25	–30.76
DUT 3	*top*	–27.25	–26.32
	bottom	–27.31	–26.50
DUT 4	*top*	–27.54	–26.21
	bottom	–27.55	–27.12

larger than those reported in [4] for SWC-based and EM-simulation test objects.[1] This increase can be assigned to measurement uncertainties and the support structure on which the DUTs were placed. While a thorough investigation is beyond the scope of this paper and will be presented in future work, first tests suggest that the support structure is the dominant source of error.

4.3 Error Distribution

While SMSE is a good metric to evaluate the overall error, it provides no information on the error distribution. To in-
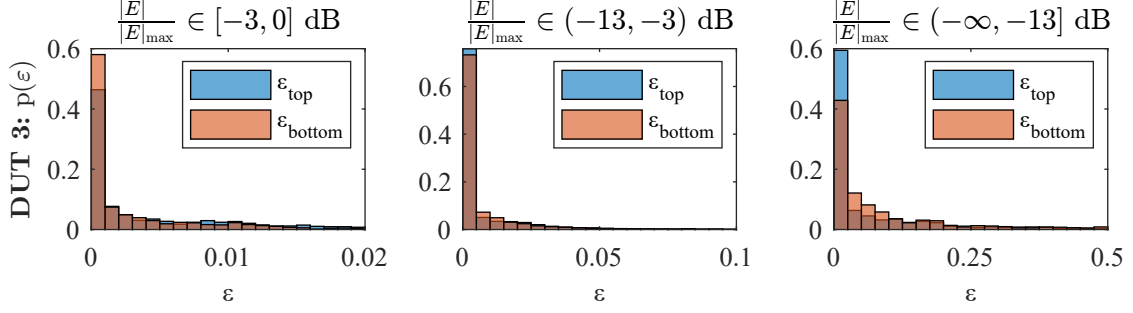
Figure 3. Normalized square error distributions: DUT 3.
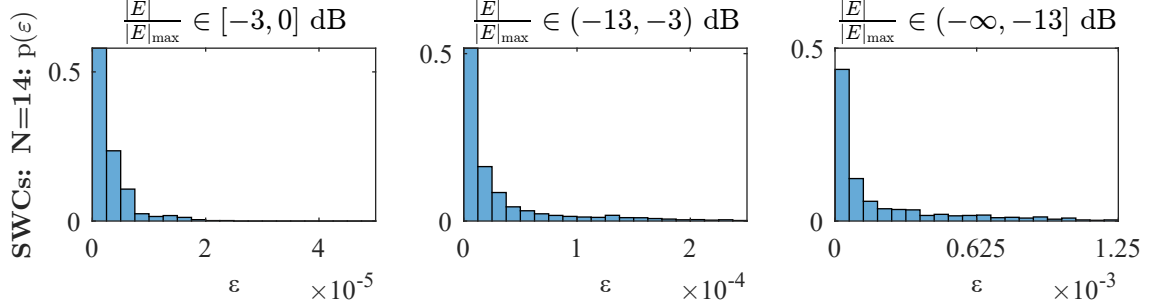
Figure 4. Normalized square error distributions: random SWCs ($N = 14$).

vestigate whether the accuracy depends on the magnitude of a measurement point, the normalized square error (NSE) distribution was evaluated, defined as:

$$\varepsilon(\chi, \theta, \phi) = \frac{|E_{\text{measured}}(\chi, \theta, \phi) - E_{\text{stitched}}(\chi, \theta, \phi)|^2}{|E_{\text{measured}}(\chi, \theta, \phi)|^2}. \quad (4)$$

Histograms of NSE distribution for three magnitude intervals were created using data of all measured frequencies. Results for DUT 3 can be seen in Fig. 3, where the range of magnitudes relative to the maximum magnitude is displayed above the corresponding histogram. Similar results were obtained for all DUTs. Looking at the histograms, one can see that the NSE distributions spread out for lower magnitude levels. As such, radiation patterns stitched with the discussed method are reliable in areas of strong radiation while radiation minima show reduced accuracy. To confirm that this behavior is caused by the method itself and not measurement noise, the distribution analysis was also done on an analytical test model of random SWCs ($N = 14$) from [4]. As can be observed in Fig. 4, the results show the same behavior, thus confirming the method's reduced accuracy at lower magnitude levels.

5 Conclusion

The truncated pattern stitching method was tested on connectorless antenna-equipped IoT devices. A measurement setup capable of characterizing used test objects was presented, along with the required adaptations of the stitching method for this purpose. Comparing weighted SMSE results of our DUTs to those presented in [4], it was seen that excluding the coaxial cable brought a small error reduction. Testing how well the processed data matches measured data

showed that the errors are more than 20 dB above the results of analytical test objects from [4]. This lead to the conclusion that even a low-permittivity ROHACELL® support structure plays a much larger role in stitching errors than initially expected. Additionally, a normalized square error distribution analysis was carried out on the obtained data. The analysis has shown that large magnitudes are represented with high accuracy, while minima in the pattern are more prone to error when using this truncated pattern stitching method.

References

[1] E. Martini, S. Maci, and L. J. Foged, "Spherical near field measurements with truncated scan area," in *Proceedings of the 5th European Conference on Antennas and Propagation (EUCAP)*, 2011, pp. 3256–3258.

[2] R. Cornelius, H. Shakhtour, and D. Heberling, "Extrapolation of truncated spherical near-field measurements," in *2012 42nd European Microwave Conference*, 2012, pp. 301–304.

[3] J. Soklič and H. Arthaber, "Investigation of coordinate system rotation and translation on iteratively reconstructed truncated antenna field patterns," in *2022 IEEE International Symposium on Antennas and Propagation and USNC-URSI Radio Science Meeting (AP-S/URSI)*, 2022, pp. 631–632.

[4] ——, "Full-sphere characterization of low-gain antennas via truncated field pattern stitching," in *2022 Antenna Measurement Techniques Association Symposium (AMTA)*, 2022, pp. 1–6.